Dirasat: Human and Social Sciences, Volume 49, No. 6, Supplement 1, 2022

Deanship of Scientific Research

Detection of the Land Surface Temperature Changes in Ma'an Governorate using Remote Sensing Data during the Period (1990-2018)

Aymen Taani[1]*, Yusra Al-Husban[2]

[1] Department of Applied Geography, Faculty of Arts and Humanities, Al al-Bayt University, Jordan.

[2] Department of Geography, School of Arts, The University of Jordan, Amman, Jordan.

Received: 27/7/2021
Revised: 7/9/2021
Accepted: 17/10/2021
Published: 30/12/2022

* *Corresponding author:*
aymentaani123@yahoo.com

Citation: Taani, A., & Al-Husban, Y. (2022). Detection of the Land Surface Temperature Changes in Ma'an Governorate using Remote Sensing Data during the Period (1990-2018). *Dirasat: Human and Social Sciences*, *49*(6:), 358–366. https://doi.org/10.35516/hum.v49i6:.4034

Abstract

This paper investigates multi-temporal land surface temperature (LST) for large ungauged areas of Ma'an Governorate, Jordan, based on changes in normalized difference vegetation index (NDVI) using remotely sensed data. Five mosaic images were taken for both the 1990 and 2018 years by Landsat 5 (TM) and Landsat 8 (OLI) (path/row, 174/36- 174/37). These were used as the basic data source, where most of Ma'an Governorate has no meteorological stations. The five-mosaic images for both Landsat 5 and Landsat 8-OLI were taken in September. LST and NDVI maps have been generated to determine the changes in LTS during the monitoring period. The results showed that the minimum value of LST increased by 4°C, and the mean surface temperature increased nearly by 2°C between 1990 and 2018. The average LST has been rising at a rate of 0.071°C/y.

Keywords: Land surface temperature; land surface emissivity; normalized difference vegetation index.

كشف التغيرات في درجة حرارة سطح الأرض في محافظة معان باستخدام بيانات الاستشعار عن بعد خلال الفترة 1990-2018

أيمن الطعاني[1]*، يسرى الحسبان[2]

[1] قسم الجغرافية التطبيقية، كلية الآداب والعلوم الإنسانية، جامعةآل البيت، الأردن.

[2] قسم الجغرافية، كلية الآداب، الجامعة الأردنية، عمان، الأردن.

ملخّص

تبحث هذه الورقة في درجة حرارة سطح الأرض متعددة الأزمنة (LST)للمناطق الواسعة في محافظة معان، الأردن، استنادًا إلى التغيرات في مؤشر الغطاء النباتي (NDVI) باستخدام بيانات الاستشعار عن بعد.جربالتقاط خمس صور فضائية لكل من عامي 1990 و 2018 بواسطة الاقمار الاصطناعية Landsat 5 (TM) و Landsat 8 (OLI) مسار /صف، 36- / 174 174/37). جرى استخدام هذه البيانات كمصدر أساسي للبيانات؛ حيث لا توجد محطات أرصاد جوية في معظم محافظة معان..جرى التقاط الصور المكونة من خمس صور فضائية لكل من لاندسات 5ولاندسات 8-OLI في سبتمبر، وأنشئت خرائط LST و NDVI لتحديد التغييرات في LTS خلال فترة المراقبة. أظهرت النتائج أن الحد الأدنى لقيمة LSTزاد بمقدار 4درجات مئوية، وزاد متوسط درجة حرارة السطح بمقدار 2 درجة مئوية تقريبًا بين عامي 1990 و2018. وقد ارتفع متوسط LST بمعدل 0.071 درجة مئوية /سنة.

الكلمات الدالة: درجة حرارة سطح الأرض، إشعاعات سطح الأرض، مؤشر الغطاء النباتي.

1. Introduction

Satellite remote sensing became a proper source and technique for estimating LST, as it is key element in the management of resources (Mallick, et al, 2008; O'Donnell, 2001; Price, 1983; Ayanlade, 2017; Anderson, 1997; Sobrino and Raissouni, 2001). The LST in ungauged semi-arid to arid areas is considered among the important of challenges (Choudhury, et al, 1994; Al-husband and Zghoul, 2017; Chander, and Groeneveld, 2009). The LST varies with changes in climatic conditions and human activities, where prediction accuracy becomes challenging, particularly in arid areas (Al-husband and Zghoul, 2017). In this study, Landsat 5 and 8 TIRS Data satellite data have been used to estimate the LST for Ma'an based on NDVI index (Schmugge et al, 1998; GU and Gillespie, 2000; Orhan and Yakar, 2016; Weng et al, 2004). The NDVI can provide details about the spatial distribution of vegetation (Yan et al, 2002). The NDVI and LST were used in several categories (Mallick, et al, 2008; McMillin, 1975). This work is intended to estimate the LST of large ungauged area with scarce geospatial information (AL-Taani et al, 2021).

2. Methodology

2.1. Study area

Ma'an, a semi-arid to arid area, it extends between °35 ′30 to °38 ′00 E longitude and °29 ′00 to °31 ′30 N latitude, (Figure 1). With an area of 33477 km², Ma'an is the largest governorate in Jordan representing about 37% of the country's land area. The desert climate is predominant in Ma'an, except for small area in the western highlands where the Mediterranean climatic conditions prevail. It is characterized by rare and intermittent rainfall ranging from < 50 mm (in the eastern, northern and central Ma'an) to 350 mm in the western highlands (about 163.05km² representing about 0.49 %.

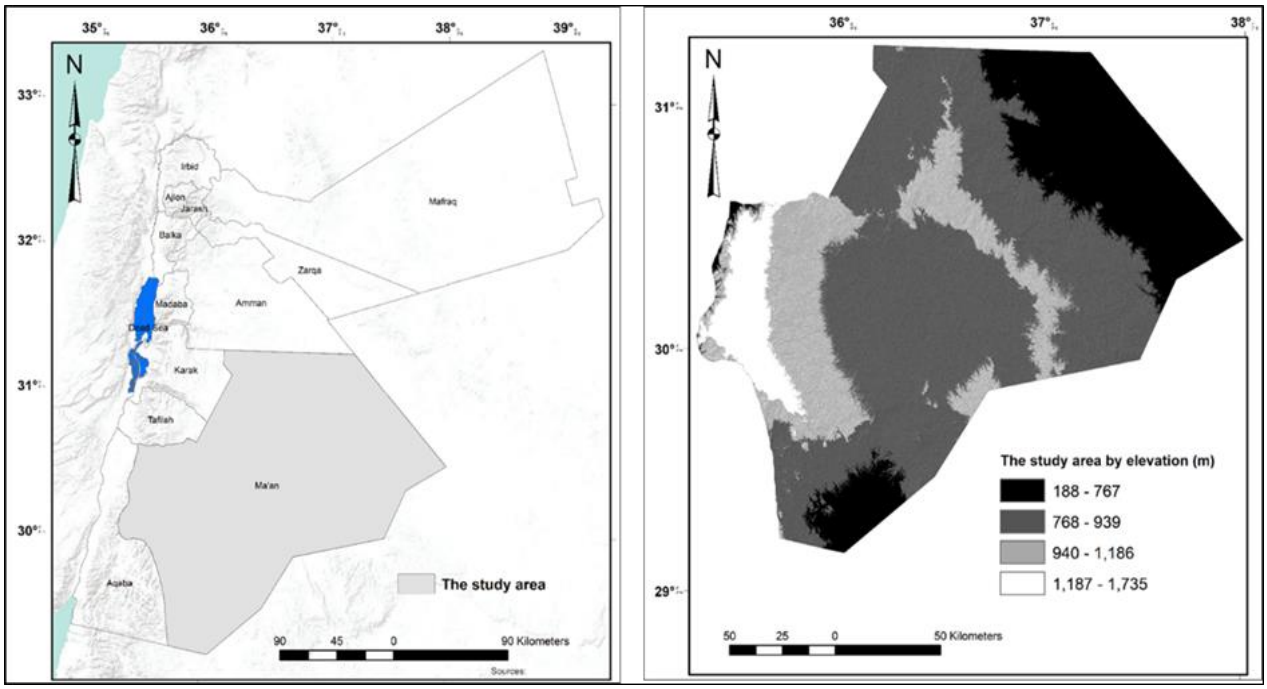

Figure 1. The location of Ma'an Governorate in Jordan, with elevation (m) extracted from ASTER DEM.

The study area varies in topography, with ground surface elevations varying between 257 m in the central part, and 1735 m in the western highlands with an average elevation of 996m. About 77.8% of the area has an elevation that varies from 262 m to 932 m (Table 1).

Table 1.The spatial distribution of elevation (m).

Elevation classes (m)	Area (KM²)	Area (%)
257- 706	4986.583	14.9
707-837	6843.104	20.5
838-977	16189.908	48.3
978-1219	3849.74	11.5
1220-1735	1606.848	4.8
Total	33476	100

2.2. Data sources and processing

The study area is covered by 5 Landsat images for each year 1990 and 2018. Image acquisition and pre-processing, for derivation of LST images, were extracted from Landsat 5 and Landsat 8. Images of Landsat 5 and Landsat 8 with meta data (MTL) files were free downloaded from the United States Geological Survey website (USGS) website. https://glovis.usgs.gov (USGS, 2019), cloud free Landsat 5 and Landsat 8 were selected in September for this study. Five satellite images covered the study area for 1990 and 2018 (from 9-17/September/1990, and Landsat 8 from 17-26/September/2018). Landsat 5 and 8 were pre-processed to create LST maps for 1990 and 2018. Description of the steps and procedures adapted in the study is presented in Figure 2.

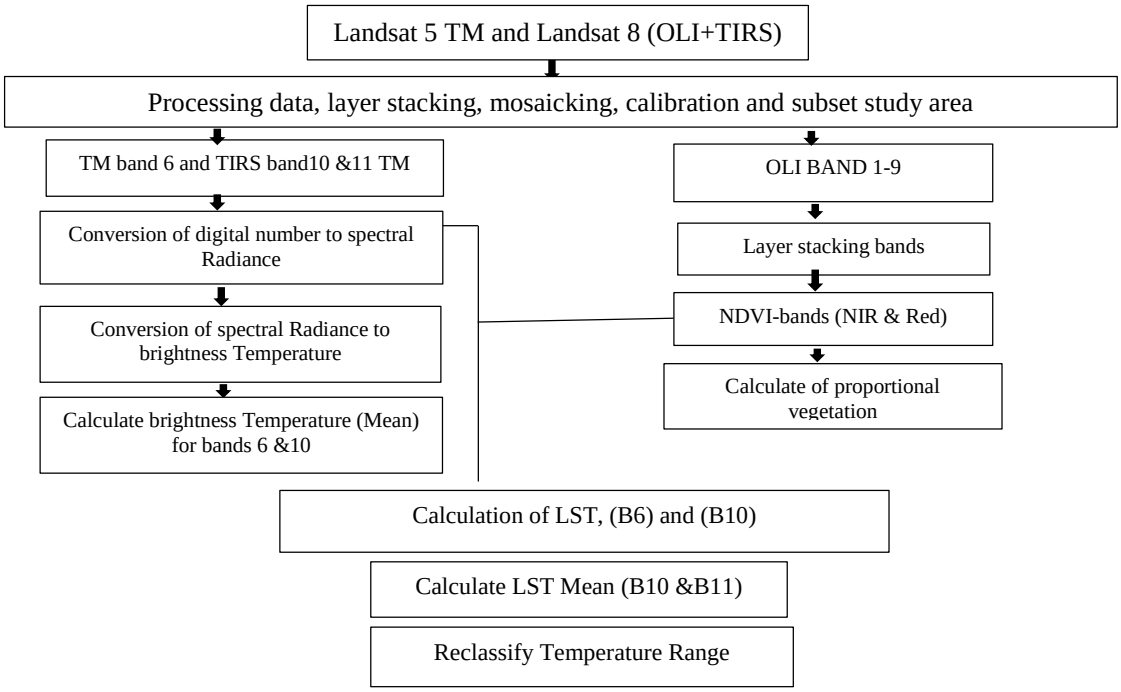

Figure 2: Flow chart of the methodology.

ArcMap software was used to combine the visible and near infrared (NIR) bands and create stacking layers. Landsat were corrected using ground features such as road crosses, before the Landsat images were mosaicked, subset and clipped to the borders of the study area (Al-husban, 2017; Farhan and Al-Bakri, 2012). The Landsat images used multi-bands with varying wavelengths (Barsi et al, 2014), as presented in Table 2.

Table 2: Specifications for Landsat TM and OIL bands used in this study.

Bands _1990	Wavelength (micrometers)	Resolution (meters)
Band 1 – visible blue	0.45-0.52	30
Band 2-Green	0.52-0.60	30
Band 3-Red	0.63 - 0.69	30
Band 6 Thermal infrared	10.40 - 12.50	30
Bands_2018	Wavelength (micrometers)	Resolution (meters)
Band 4 – Red	0.636 - 0.673	30
Band 5 - Near Infrared (NIR)	0.851 - 0.879	30
Band 10 - Thermal Infrared (TIRS) 1	10.60 - 11.19	30

A cloud-free Landsat 5 and 8 images (path/row= 174/36- 174/37), acquired for September 1990 and 2018, were utilized to generate LST maps. For image-processing, remote sensing data were transformed to real-world coordinates using UTM projection and WGS 84 datum. LST images were extracted from Landsat 5 thermal band (6) and Landsat 8 thermal band (10). The NDVI derived from Landsat red and near-infrared bands were used to estimate fractional vegetation cover. Then it was used to estimate emissivity for Landsat thermal bands. The Landsat-5 Band 6 and Landsat-8 Band 10 where used to calculate brightness temperature. The wavelengths of the thermal bands for both Landsat 5 and Landsat 8 were 10.40 – 12.50A micrometers. Details of the Landsat sense are listed in table 2. In this study, the methodology involves preparing NDVI and Land surface temperature maps following Meta (MTL) data values, used in the calculation. Conversion of Digital Number (DN) to spectral radiance (Lλ), DN of a pixel in an image is a numerical indicator representing the pixel brightness in that image. Each pixel of the Landsat images was converted from DN to Lλ. The workflow is summarized in Figure 2.

2.2.1. Estimation of LST from Landsat-5

Thermal infrared band data, Band (6) of Sept 9-17-1990**,**

and DN of sensors were converted to spectral radiance to estimate LST from Landsat-5, using equation (**Eq**. **1**) (Chander and Groeneveld, 2009),1260.56 / (log ((607.76)/ (15.303 - 1.238) / 254)*($n1_l5_1990 -1) +1.238)) +1)) - 273.15 (C^o) percent degree temperature

Temperature = K2 / (Log)/ (k1/Radiance) +1)

Radiance = (^{L}max-^{L}min)/ (Qcal max-Qcal min)

Radiance= (^{L}max-^{L}min) /254)*(DN-1) +Lmin)

K2 = 1260.56

K1 = 607.76

Temperature (C^o) = 1260.56 / (log (607.76)/ (15.303-1.238)/254)*(Raster-1) +1.238) +1) Kalvin degree.

where the **Lλ** is the cell value as radiance ($W*sr^{-1}*m^{-2}$), Qcal is the quantized calibrated digital number, Qcal min is the minimum quantized calibrated pixel value, and Qcal max is the maximum quantized and calibrated data digital number; LMINλ is the spectral radiance scales to Qcal min, LMAXλ is the spectral radiance scales to Qcal max,(**Eq.2**.).

$$\mathbf{L\lambda = (Lmax\lambda - Lmin\lambda)/(Qcal\ max - Qcal\ min)\ \times (Qcal - Qcal\ min) + Lmin\lambda}$$

where the Lλ is the cell value as radiance ($W \cdot sr^{-1} \cdot m^{-2}$), Qcal is the quantized calibrated digital number, Qcal min is the minimum quantized calibrated pixel value, and Qcal max is the maximum quantized calibrated pixel value; LMINλ is the spectral radiance scales to Qcal min, LMAXλ is the spectral radiance scales to Qcal max.

2.2.2. Estimating the LST from the Landsat 8

LST was estimated from Landsat-8 thermal infrared band data, in which DN of sensors were converted to spectral radiance using the following equations (John et al, 2018);

1. Top of Atmosphere (TOA) Radiance:

Using the radiance-rescaling factor, Thermal Infra-Red Digital Numbers can be converted to TOA spectral radiance, (**Eq.3**)

$$L\lambda = ML * Qcal + AL$$

Where:

$L\lambda$ = Spectral radiance ($W \cdot sr^{-1} \cdot m^{-2}$)

ML = Radiance multiplicative scaling factor for the band (Radiance_Mult_Band_n from the metadata)

AL = Radiance additive scaling factor for the band (Radiance _Add_Band_n from the metadata)

Qcal = Level 1 pixel value in DN

2. Top of Atmosphere (TOA) Brightness Temperature:

Spectral radiance data can be transferred to TOA brightness temperature using the thermal constant values in Meta data file, (**Eq.4**).

$$BT = K2 / \ln (k1 / L\lambda + 1) - 272.15$$

BT = Top of atmosphere brightness temperature (°C)

$L\lambda$ = Top of atmosphere spectral radiance (Watts/(m2*sr * μm))

K1 = K1 Constant Band (No.)

K2 = K2 Constant Band (No.)

3. Normalized Differential Vegetation Index (NDVI):

The Normalized Differential Vegetation Index (NDVI) is a standardized vegetation index estimated using NIR (Band 5) and Red (Band 4) bands, as per the following equation (**Eq.5**).

$$NDVI = (NIR – RED) / (NIR + RED)$$

Where:

RED= DN values from the RED band

NIR= DN values from Near-Infrared band

4. Land Surface Emissivity (LSE):

Land surface emissivity (LSE) is the mean emissivity of an element of the Earth surface calculated from NDVI values (**Eq.6**).

$$PV = [(NDVI – NDVI\ min) / (NDVI\ max + NDVI\ min)]^2$$

Where:

PV = Vegetation Proportion

NDVI = Digital Number values from NDVI Image

NDVI min = Minimum Digital Number values from NDVI Image

NDVI max = Maximum Digital Number values from NDVI Image

$$E = 0.004 * PV + 0.986$$

Where:

E = Emissivity of Land Surface

LST: Land Surface Temperature, which is the radiative temperature, calculated using top of atmosphere brightness temperature, emitted radiance wavelength, emissivity of land surface,(**Eq.7**).

$$LST = (TB/1) + W*(TB/14380) * \ln(E)$$

Where:

TB = Top of atmosphere brightness temperature (°C)

W = Emitted radiance wavelength

Where:

$$T = \frac{Tb}{1 + \left(\lambda \times \frac{Tb}{\rho}\right) LN\ \delta\ \lambda}$$

T = Top of atmosphere brightness temperature (K)

Lλ = Top of atmosphere spectral radiance (Watts/(m2 * srad * μm)

K1 = Band-specific thermal conversion constant from the metadata (K1_CONSTANT_BAND_x, where x is the thermal band number)

K2 = Band-specific thermal conversion constant from the metadata (K2_CONSTANT_BAND_x, where x is the thermal band number).

Emissivity of Land surface (LSE) is the mean emissivity of an element of the surface of the Earth calculated from NDVI values. The land surface emissivity (LSE (ε)) should be known to calculate LST. The emissivity of ground is conditionally calculated as per Zanter (2018), (**E.q.8**).

$$\varepsilon\lambda = \varepsilon v\lambda Pv + \varepsilon s\lambda(1 - Pv) + C\lambda$$

where εv and εs are the emissivities of vegetation and soil, respectively, Cλ average surface roughness (for a flat surface C is equal 0). In this study, LSE (ε) extracted using NDVI value of 0.966 taking into account the condition of bare soil. Vegetation Proportion (PV) (Calvet, and Julien, 1996;Wang et al,2015), suggests the use of NDVI values for soil (NDVIV = 0.5 and NDVIs = 0.2) to apply in global conditions..

3. Results and Discussions

3.1. Analysis of NDVI; The spatial distribution of NDVI values from the Landsat TM and Landsat 8 images is presented in Figure 3. The NDVI of 1990 values varied between –0.2 and 0.63, whereas the NDVI of 2018 ranged from –0.3 to 0.6.

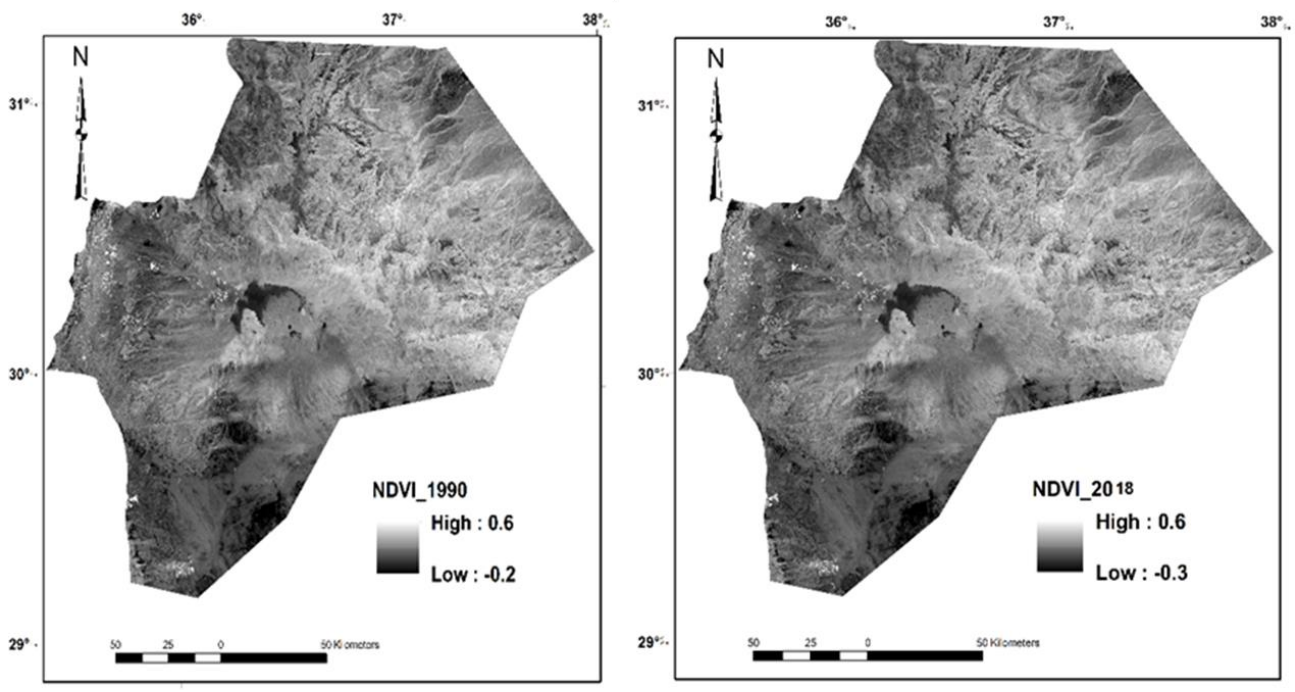

Figure 3 NDVI maps for1990 and 2018, respectively.

High NDVI values were observed in the southwestern part of the study area, whereas lower values and the bare ground have been detected in the majority of Ma'an. The maximum NDVI values decreased from 1990 to 2018 by -0.05. The vegetated area (of the different years) showed that there has been a considerable vegetation cover decreased by 108.03km² (Figure 4 and Table 3). Ma'an Governorate consists mostly of uncultivated land of 33304.66km² (99.49%), and the forest and irrigated areas varied between 108.06km² (0.32%) and 102.68km² (0.31%) from 1990 and 2018, respectively. The low NDVI value is probably attributed to infertile soil, and scarcity of water (AL-Taani, et al, 2018).

Table 3. LULC changes in different categories during the monitoring period (AL-Taani et al, 2018).

LULC-1990			LULC_2018		
OBJECTID	Land use/Cover class	Area (km^2)	Area (%)	Area (km^2)	Area (%)
1	Forest and Irrigated area	86	0.25	102.68	0.31
2	Built-up area	24	0.074	68.66	0.21
3	Bare land	33366	99.67	33304.66	99.49
	Total area	33476	100	33476	100

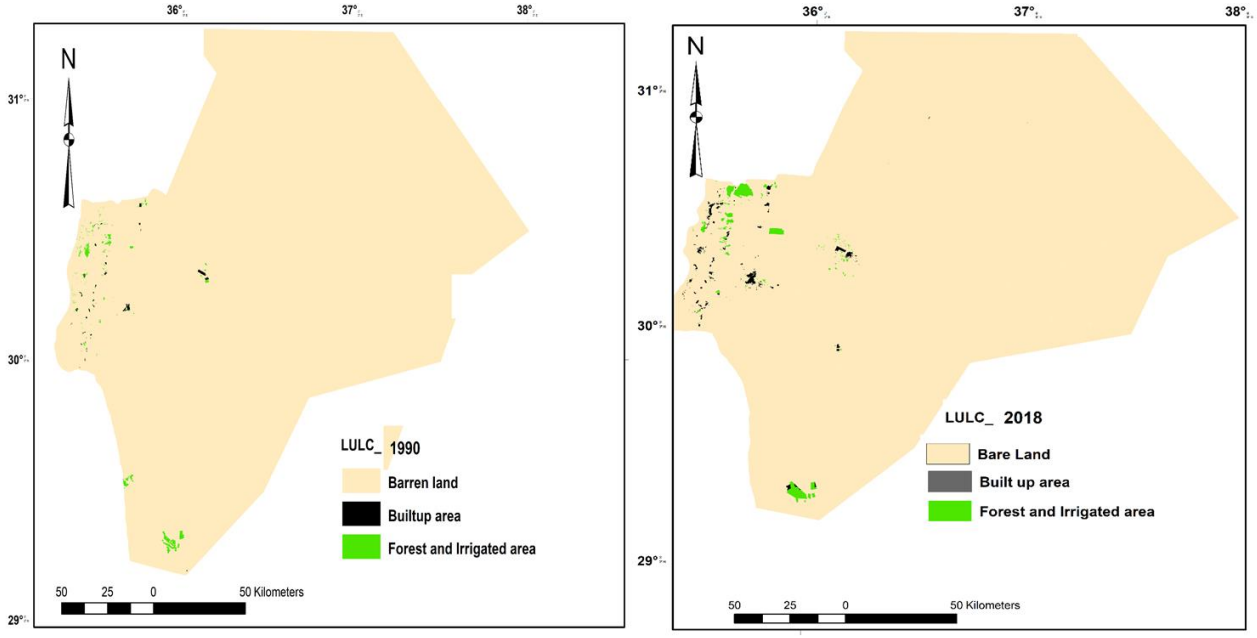

Figure 4. (LULC) changes in different categories during the monitoring period. Data source (AL-Taani, et al, 2021).

3.2. Land surface temperature changes

Band TM6 is located in the range 10.40–12.50 Am and band 10 is located in the range of 10.60 - 11.19. The minimum temperature value has increased by 4°C with an average of 0.143°C/year, and the mean temperature increased by 3°C at an increasing rate of 0.071°C per/year. Figure 4 shows the spatial distribution of the LST in 1990 and 2018. LST values varied between 16°C and 34°C (with a mean value of 25°C) in 1990. However, in 2018, the LST of 2018 ranged from 20°C to -36°C (with an average value of 28). The maximum change (43%) of LST was recorded in various parts of the eastern and southwestern Ma'an. The spatial distribution of LST changes showed that about 81.3% of the total area of Ma'an Governorate are with temperatures varied between 20°C and 27°C in 1990. In 2018, however, about 79.9% of the total area of Ma'an showed a temperature ranging from 27-30°C (Table 4). The vegetated area in Ma'an Governorate has no significant effect on the land surface temperature modify, as it represents a small and clustered irrigated areas.

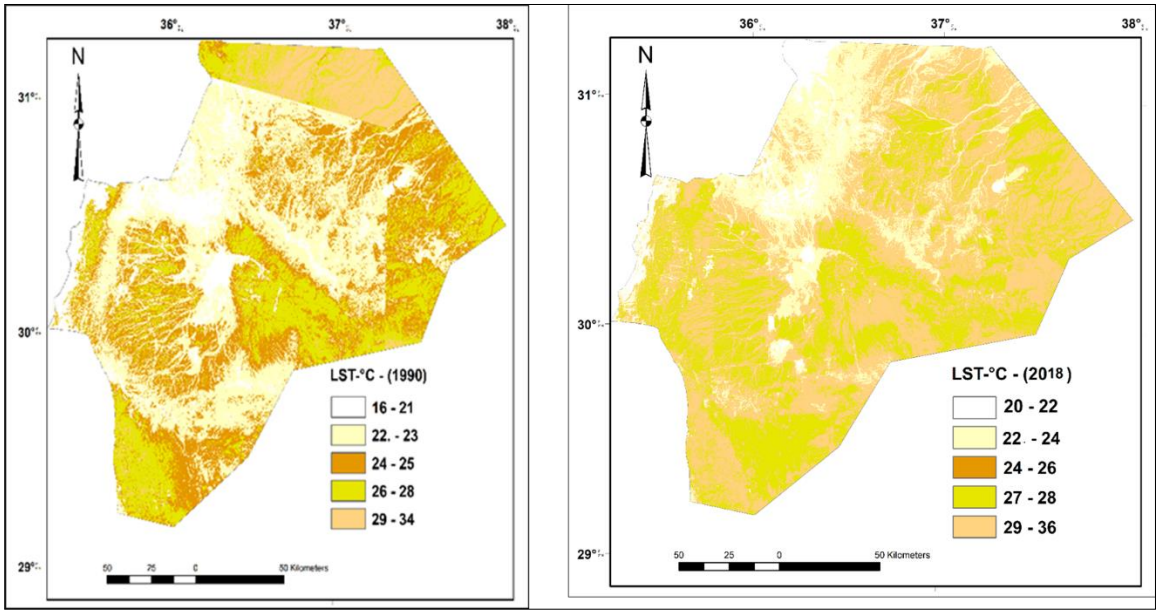

Figure. 5. Spatial distribution of LST during the study period.

Table 4. Statistics of the spatial distribution of LTS during the study period.

LST_1990	Area (km²)	Area percentage (%)	LST_2018	Area (km²)	Area percentage (%)
16-21°C	1640.4	4.9	20-21°C	13.39	0
21-23°C	13524.7	40.4	22-24°C	382.3	1.2
23-27°C	13692	40.9	24-26°C	6358.1	19
27-30°C	4084.2	12.2	27-28°C	26719.87	79.8
30-34°C	0.0256	1.6	29-36°C	3.51	0.05
Total	33477	100		33477	100

4. Conclusions

Landsat 5 band 6 and OIL 8 band 10 were employed to estimate the brightness temperature, while bands 3, 4 and 5 were used to generate NDVI. The average value of LST of Ma'an increased by 3°C during the study periods (1990 to 2018). Overall, the average LST was increasing at a rate of 0.071°C/year. In addition, the results revealed that the vegetation cover has increased (as indicated by NDVI), though the study area has suffered increasing rates of desertification. Even in the western highlands with a Mediterranean climate, the LST the minimum LST increased from 16°C to 20°C during the monitoring period.

References

Al-Husban, Y., and Zghoul M., (2017), Analysis of Drought Patterns in Azraq Depression (AD), During the Period (1984-2016) In: International Journal of Applied Environmental Sciences, 12(2): pp. 341-358.

Al-Husban Y, (2017).Comparison of Accuracy of Two Global DEMs, and the Extracted DEM from the Topographic Map of the Tafilah Governorate, Journal of Earth Science and Engineering 7 , 230-241.

Alavi Panah, S. K. (2003). Study of Surface Temperature the Lut Desert Based upon Landsat Thermal Band and Field Measurement, Biaban, 7 (2): 67-79.

AL-Taani, A. Al-husban, Y. and Farhan, I. (2021). Land use/cover classification, change detection and Land suitability evaluation

for agricultural land-use planning in Ma'an/Jordan. Egyptian Journal of Remote Sensing and Space Science vol.24, 109-117.

Anderson, H. S.(1997). Land surface temperature estimation based on NOAA-AVHRR data during the HAPEX-Sahel experiment. Journal of Hydrology, 189, 788-814.

Ayanlade, A. (2017). Remote sensing approaches for land use and land surface temperature assessment: A review of methods. Int. J. Image Data Fusion 2017, 8, 188–201, doi:10.1080/19479832. 1299802.

Barsi, J. A. Schott J. R. Hook S. J. Raqueno N. G. Markham B. L. Radocinski R. G., (2014). "Landsat-8 thermal infrared sensor (TIRS) vicarious radiometric calibration," Remote Sensing, vol. 6, no. 11, pp. 11607–11626.

Choudhury, B. J., Ahmed, N. U., Idso, S. B., Reginato, R. J., & Daughtry, C. S. T. (1994). Relations between evaporation coefficients and vegetation indices studied by model simulation. Remote Sensing of Environment, 50, 1 – 17.

Calvet, J.-C., and Julien, J.-P. (1996). Land surface temperature retrieval in dry conditions from infrared and microwave satellite radiometry. Remote Sensing Reviews, 13, 235-255.

Chander, G., Groeneveld, D.P. (2009). Intra-annual NDVI validation of the Landsat 5 TM radiometric calibration. International Journal of Remote Sensing, 30, 1621–1628.

Gillespie, A. R., Rokugawa, S., Hook, S., Matsunaga, T., & Kahle, A. B.(1998). A temperature and emissivity separation algorithm for Advanced Spaceborne Thermal Emission and Reflection Radiometer (ASTER) images. IEEE Transactions on Geoscience and Remote Sensing, 36, 1113–1126.

Gu, D., and Gillespie, A. R., (2000). A new approach for temperature and emissivity separation. International Journal of Remote Sensing, 21, 2127-2132.

Mallick, J., Kant, Y., and Bharath, B.D.(2008). "Estimation of land surface temperature over Delhi using Landsat-7 ETM+, J. Ind. Geophys. Union Vol.12, No.3, pp.131-140.

McMillin, L.M.(1975). "Estimation of Sea Surface Temperatures from Two Infrared Window Measurements with Different Absorption". J. Geophys. Res., 80, 5113–5117.

O'Donnell, E. (2001). LANDSAT 8 (L8) DATA USERS HANDBOOK, Department of the Interior U.S. Geological Survey USER GUIDE, Version 3.0 October 2018.

Orhan O., Yakar, M. (2016). Investigating Land Surface Temperature Changes Using Landsat Data in Konya, Turkey, The International Archives of the Photogrammetry, Remote Sensing and Spatial Information Sciences, Volume XLI-B8, 2016 XXIII ISPRS Congress, 12–19 July 2016, Prague, Czech Republic.

Price, J. C. (1983). Estimating surface temperature from satellite thermal infrared data—a simple formulation for the atmospheric effect. Remote Sensing of Environment, 13, 353 – 361.

Schmugge, T.; Hook, S.J.; Coll, C.(1998). Recovering Surface Temperature and Emissivity from Thermal Infrared Multispectral Data. Remote Sens. Environ. 65, 121–131.

Sobrino, J. A., Raissouni, N., & Li, Z. -L. (2001). A comparative study of land surface emissivity retrieval from NOAA data. Remote Sensing of Environment, 75, 256– 266.

Weng, Q.H.; Lu, D.S, Schubring, J. (2004). Estimation of land surface temperature-vegetation abundance relationship for urban heat island studies. Remote Sens. Environ. 89, 467–483.

Yan, P., Shi, P., Gao, S., Chen, L., Zhang, X., Bai, L.,(2002). 137Cs dating of lacustrine sediments and human impacts on Dalian Lake, Qinghai Province, China. Catena. 47,91–99.

Zanter, K., 2018, DATA USERS HANDBOOK, Department of the Interior U.S. Geological Survey USER GUIDE LANDSAT 8 (L8), Version 3.0.